WILEY-VCH

DOI: 10.1002/…
Article type: Full Paper

Long-Term Perfusion Culture of Monoclonal Embryonic Stem Cells in 3D Hydrogel Beads for Continuous Optical Analysis of Differentiation.

*Hans Kleine-Brüggeney, Liisa D. Van Vliet, Carla Mulas, Fabrice Gielen, Chibeza C. Agley, José C.R. Silva, Austin Smith, Kevin Chalut and Florian Hollfelder**

H. Kleine-Brüggeney, Dr L. D. Van Vliet, Dr F.M. Gielen, Prof. A. Smith, Prof. F. Hollfelder
Department of Biochemistry, University of Cambridge, 80 Tennis Court Road, Cambridge, CB2 1GA, U.K.
E-mail: fh111@cam.ac.uk

Dr C. Mulas, Dr. C.C. Agley, Prof. J.C.R. Silva, Prof. A. Smith, Prof. K. Chalut
Wellcome Trust/Medical Research Council Stem Cell Institute, Tennis Court Road, University of Cambridge, Cambridge, CB2 1QR, UK.

Prof. K.Chalut
Department of Physics, University of Cambridge, 19 J J Thomson Avenue, Cambridge, CB3 0HE, UK.

Keywords: stem cells, microdroplets, single cell analysis, hydrogels, pluripotency

Abstract

Developmental cell biology requires technologies in which the fate of single cells is followed over extended time periods, to monitor and understand the processes of self-renewal, differentiation and reprogramming. We present a workflow, in which single cells are encapsulated into droplets (Ø: 80 µm, volume: ~270 pL) and the droplet compartment is later converted to a hydrogel bead. After on-chip de-emulsification by electro-coalescence, these 3D scaffolds are subsequently arrayed on a chip for long-term perfusion culture to facilitate continuous cell imaging over 68 hours. Here the response of murine embryonic stem cells (mES cells) to different growth media, 2i and N2B27, was studied, showing that the exit from pluripotency can be monitored by fluorescence time-lapse microscopy, by immunostaining and by RT-qPCR. The defined 3D environment emulates the natural context of cell growth (e.g. in tissue) and enables the study of cell development in various matrices. The large scale of cell cultivation (in 2000 beads in parallel) may reveal infrequent events that remain undetected in lower throughput or ensemble studies. This platform will help to gain qualitative and quantitative mechanistic insight into the role of external factors on cell behavior.

1. Introduction

Microfluidic droplets,[1-3] highly monodisperse water-in-oil emulsions, provide a new format for the segmentation of single cells of bacterial[4-6] or eukaryotic[7-10] origin. When the aqueous content of the droplet is converted into hydrogel beads,[11-13] the resulting three-dimensional scaffold emulates the embedding of cell in a biological matrix.[14, 15] This hydrogel format enables the handling of single cells within a three-dimensional context as well as analysis by flow cytometry and microscopy.[16-18] This new experimental paradigm will be useful to explore the complex interplay between single cells and their responses to physical and chemical environmental stimuli.

Deciphering the heterogeneity of a cell population plays an important role in understanding the mechanisms of cellular behavior by replacing ensemble measurements with insight into the dynamics of single cells or small subpopulations.[19-21] Soluble factors, interactions between the extracellular matrix (ECM) and the cell, cell-cell interactions as well as physical influences (e.g. shear stress, matrix elasticity) collectively determine cell signaling and behavior.[22-24] For example, the 3D culture of cancer cell lines was shown to result in (i) drastic changes in gene expression profiles when compared to 2D culture and (ii) a change of phenotypic behavior upon stimulation with different drugs.[25] Pluripotent mouse embryonic stem (mES) cells also exhibited different gene expression patterns when grown in a 3D matrix [26, 27] and defined 3D microenvironments were predicted to direct stem cell lineage choice.[28, 29] The potential importance of the microenvironment and its influence on cell heterogeneity highlights the need for an experimental set-up that enables the study of single cells in a well-defined 3D scaffold and is able to reproduce biologically relevant events and timescales.

Here, we establish a workflow in which microfluidic droplets are used to compartmentalize single cells within a hydrogel matrix to study the cellular heterogeneity of separate monoclonal populations in a 3D environment over time and under different external conditions (**Figure 1**). Several building blocks of this workflow have been established previously, including cell

encapsulation into hydrogel beads using a flow focusing geometry[11-13, 30, 31] and hydrogel bead trapping and imaging.[16, 17, 32, 33]

In this work we connect single cell compartmentalization in droplets with subsequent spatial immobilization in 3D hydrogel culture by demonstrating that heterogeneity of clonal colonies can be optically investigated through time-lapse fluorescence microscopy under specific and controlled conditions relevant for the study stem cell biology .[34, 35] Firstly, we present a microfluidic device module that performs the de-emulsification of beads, enabling automation and coupling of this module to further microfluidic chips. Secondly, we introduce a chip design for the spatial immobilization and perfusion of hydrogel beads that is based on a flow dependent trapping mechanism resulting in flow-induced trapping without the need for a bypass channel.[32, 36-38] Finally, we validate our system by comparing the effect of different perfusion media on the development of mES cells using time-lapsed confocal microscopy and show the compatibility of the hydrogel bead format with immunohistochemistry and RT-qPCR.

2. Results

2.1. Single Cell Encapsulation into Hydrogel Beads

Single cell encapsulation was performed as described previously.[11-13] Briefly, monodisperse microdroplets of low-melting point agarose with a diameter of 80 ± 4 µm (~270 pL) were produced in a flow focusing chip made by soft lithography in PDMS (**Figure S1**). Directly after encapsulation, droplets were collected on ice to allow for gel formation, thus producing hydrogel scaffolds for proliferation in 3D culture conditions. The beads were subsequently extracted from the oil phase into a culture medium phase. For performing cell-based assays, it is essential that this de-emulsification step does not affect cell viability. Chemical de-emulsification (using weak surfactants such as perfluorooctanol, PFO) was avoided by using weak electric fields (10 ms at < 5.10^5 V/m) to initiate electro-coalescence between the microdroplet beads and an aqueous phase.[39] To this end, a microfluidic chip with two intersecting channels was constructed: one containing the droplet emulsion and a second containing an aqueous stream (Figure S1, **Video S1**).[40, 41] The two immiscible fluids form an interface at which the coalescence between microdroplets and the aqueous phase can occur. To increase interface stability we applied different surface coatings to the two microfluidic channels – one hydrophilic and one fluorophilic – using UV-induced graft polymerization (as described:[42]) the microfluidic channel for the aqueous phase was coated with poly(acrylic acid) (PAA), while the other channel was coated with trichloro(1H,1H,2H,2H-perfluorooctyl)silane (PFOTS)(**Figure S2**). These hydrophilic (PAA) and fluorophilic (PFOTS) coatings increased the wettability between the aqueous or fluorinated oil (HFE-7500) in their respective channel surfaces. In comparison to the untreated PDMS chip, the differential coating improved the operational window of the chip 4-fold (**Figure 2A and Figure S8**), allowing more flow rate pairs that stabilised the flow pattern and phase interface. Typically, PAA grafts yield a water contact angle of 60 to 70 degrees.[42] By contrast, native PDMS has a water contact angle of 104° [11] and a water contact angle of 110° was reported for silicon substrates coated with PFOTS.[43] Medium is flowed through the aqueous channel and the oil stream is generated by two

oil flows – one containing gel droplets and a second for sheath fluid to space out the hydrogel droplets (Figure S1). We measured the extraction efficiency as the ratio between the number of droplets merging with the aqueous phase and the total number of droplets passing the interface of the extraction chip, as a function of the applied voltage (**Figure 2B and C**). The extraction efficiency increased with increasing voltage amplitude and thus increasing field strength. The ideal extraction efficiency (100%, within error) was reached at sheath fluid flow rates of 5, 30 and 60 µl/min for voltages of 40, 50 and 100 V_{pp}, respectively - at a constant total flow rate of the aqueous and oil phases. An increase of the sheath fluid flow rate resulted in a decrease of the extraction efficiency at the same voltage amplitude **(Figure 2B)**. This observation can be explained by a scenario in which the sheath fluid acts as an insulating layer between droplets and the aqueous phase[44] that becomes thicker with higher sheath fluid flow rates. These higher rates required an increased electric field strength for initiating electro-coalescence, which would explain the observed decrease of the extraction efficiency, coupled with a concomitant decrease in residence time (see SI, **Figure S7**). In comparison to previous studies, the differential coating of the two channels resulted in a pronounced decrease of the voltage needed for inducing electro-coalescence by more than an order of magnitude, from >1.5 kV [40] to 50 V_{pp} (**Figure 2B**), presumably due to a decrease of the impedance of the PDMS. Such coating also improved the stability of the interface between the two fluids and thus reduced the transfer of oil into the 'recovery' medium phase used for cell culture - thereby minimising contaminants (e.g. surfactant, oil) in the growth medium to which stem cells in particular are very sensitive.[45]

Next, we investigated the effect of the encapsulation and on-chip de-emulsification processes on the viability of mES cells. To do so, we encapsulated mES cells into agarose hydrogel beads and tested the effect of different de-emulsification strategies. In-line de-emulsification of beads was performed by connecting the flow focusing microfluidic chip with the on-chip de-emulsification device via ~10 cm of tubing coiled around a 2 cm diameter plastic tube immersed in ice water. Cell viability was assessed by live/dead flow cytometry based on calcein/ethidium homodimer staining (see SI for

details). The on-chip de-emulsification did not affect cell viability (**Figure 2D** and **Figure S3**), based on cell growth and reporter gene expression as readouts.[46, 47] In comparison, the de-emulsification using the fluorosurfactant PFO (as described above and in the SI) resulted in dramatically lower cell viability that decreased by an order of magnitude with increasing amount of PFO to survival rate of ~10% with 100% PFO. Consequently, the on-chip de-emulsification using the developed extraction chip obviates the need for a chemical de-emulsifier, avoiding its detrimental effects on cell survival while facilitating integration of a de-emulsification step into automated workflows.

2.2 Hydrogel Bead Immobilization

For the long-term culture of encapsulated mES cells, a microfluidic chip was designed to spatially immobilize the hydrogel beads, while perfusing them with fresh medium. Continuous long-term tracking of stem cells has been shown in bulk 3D hydrogel layers for 40 to 100 hrs [34, 48, 49] However the monitoring of single ES cells and their clonal offspring in a way that maintains clonal identity has not yet been shown and is realized here in microfluidic hydrogel beads that perpetuate the initial droplet compartmentalization. We aimed to perform perfusion culture in combination with time-lapsed confocal microscopy to track single cells over 68 hrs and to study the formation and growth characteristics of monoclonal stem cell spheroids within their 3D hydrogel microenvironment. To this end, we developed a microfluidic chip with four channels of 500 traps each for immobilization of hydrogel beads in a precise spatial arrangement (**Figure S4**). We evaluated two trap geometries that offered an opening of either 41 µm or 58 µm through which the hydrogel beads enter the trap (**Figure 3**, Figure S4C). Because the hydrogel bead diameter was approximately 80 µm it had to be squeezed into the trap by hydraulic pressure. Both trap designs were evaluated for their trapping efficiency as a function of the flow rates used (Figure 3B). To do so, the trapping chip was perfused with the same volume (20 µl) of the bead solution (50 beads/µl)

while the flow rate was varied between 5 and 150 µl/min, and 174 traps were observed for each condition. The beads first lodge themselves in front of the trap, forcing the next bead to bypass the first bead and block the entrance of the next trap; above a given flow rate, the bead is squeezed into the trap (**Figure 3A**). Each trap was sequentially occupied by a bead (either lodged at the opening or fully trapped). The trapping efficiency was calculated as the ratio between the number of beads captured inside a trap and the total number of observed traps (**Figure 3C**). For both designs it increased with increasing flow rate and a sigmoidal behaviour was observed (Figure 3B). A trap opening of 41 µm required a 2.2-fold higher flow rate to achieve 100% trapping efficiency within error than a trap opening of 58 µm. Thus, the extent to which hydrogel beads were deformed correlated with the minimal flow rate necessary to achieve 100 % trapping efficiency. Different hydrogel compositions (e.g. type of polymer, percentage) will affect elasticity of the bead and thus change the optimal trapping flow rate. Control of the flow rate provided means to govern whether the beads were deposited in front of the trap, bypassed them or whether they were lodged in the trap. At low flow rates (<25 µl/min for a trap opening of 58 µm and <100 µl/min for a trap opening of 41 µm) hydrogel beads (1.5% w/v) were positioned in front of the traps but did not enter and a higher hydraulic pressure (induced by higher flow rates) was required to squeeze the beads into the traps (**Figure 3B and C**). The hydrogel beads can be sequentially trapped until the entire chip is filled, which is important to prevent any bead loss (**Video S2**). This trapping method differs to previous studies,[8, 36] in which hydrodynamic trapping was based on the ratio of the volumetric flow rates between a trapping and a bypass channel. Here, the hydrodynamic trapping is based on the kinetic energy of the hydrogel beads and the hydraulic pressure field that are a function of the flow rates and on the physical parameters of the bead (size and deformability of the hydrogel). Reversing the flow offered the possibility of removing and collecting the beads.

2.3 Perfusion Culture and Analysis of Monoclonal Stem Cell Spheroids under Two Different conditions

Establishing culture conditions that maintain self-renewal is an essential validation step when the influence of soluble compounds or the 3D microenvironment on stem cell behaviour is studied. We evaluated the suitability of the trapping chip for perfusion culture and clonal propagation of encapsulated mES cells by testing alternative conditions known to support self-renewal or differentiation, respectively: one lane of the chip was perfused with the medium containing 2i, which maintains pluripotency[50] and another was switched to the base medium N2B27 (lacking the 2i inhibitors mitogen-activated protein kinase signalling and glycogen synthase kinase-3 (GSK3).[51, 52] In conventional adherent culture in N2B27 without 2i, ES cells rapidly stop expressing pluripotency markers and begin to differentiate. Loss of Rex1GFP expression is an early marker of this transition.[52-54] To monitor the pluripotent state of cells, we used the RGd2 mES cell line that expresses a destabilized GFP under control of the Rex-1 promoter and down-regulates GFP expression abruptly as the cells exit the ES cell state.[47, 55] For the evaluation of the trapping chip, mES cells were encapsulated in 1.5% w/v agarose hydrogel beads, spatially immobilized into the traps described above and perfused with either 2i or N2B27 media. Cell concentrations were chosen to encapsulate single cells under Poisson distribution conditions,[4] i.e. 60% containing one, 10% two and 30% no cells. The loaded trapping chip was imaged using time-lapse confocal microscopy under growth-promoting controlled atmosphere (37 °C, 7% CO_2) (**Figure 4A**). In total, 24 traps and 28 traps containing agarose beads with single mES cells were imaged every hour for 68 hours for the 2i and N2B27 media respectively (13 of each are shown in Fig. 4). Because we chose a high time and Z-axis resolution, the number of monitored hydrogel beads was limited by the speed of image capture using the confocal microscope setup. However, the throughput could be increased using high-content screening platforms and optimising the imaging parameters. Cells cultivated in 2i maintained GFP expression over the entire imaging and culture period (68 hours) indicating that the 3D microenvironment acted as an inert scaffold without inducing stem cell differentiation.

Indeed, culturing the mESCs in our device shows a significant 3-fold improvement in cell proliferation with 62% of single cells forming colonies (and 48% growing slowly and dying), when in 2D cultures mES cell colony formation rate is merely 17%.[56, 57] By contrast, mES cells cultivated in N2B27 exhibited down-regulation of GFP expression (~15 hours) and altered colony morphology was apparent (after 30 h; **Figure 4**). This result suggests that mES cells cultivated in N2B27 exit pluripotency, as expected due to an autoinductive stimulation of the mitogen activated protein kinase (ERK1/2) pathway by FGF4 in this medium.[50, 58, 59] For the majority of trapped cells (71%, 17 of 24) growth, proliferation and spheroid formation could be observed (Figure 4, **Video S3**), matching the clonogenic efficiency observed in adherent cultures.[53] Similar to PEG-based gels,[60] 13% of cells (3 of 24) migrated through the hydrogel and escaped from the agarose bead (**Video S4**) and 17% (4 of 24) did not survive the first 15 h and were not able to form a spheroid (**Video S5**).

Next, we determined the growth rate of single, clonal-derived stem cell spheroids by quantifying GFP expression over time for each bead by computing the pixel intensity of different Z-stacks (Figure 4B). The cumulative fluorescence intensity exponentially increased over time. Furthermore, we could quantify the doubling time for each generation of cells with a mean value of 22.8 h ± 10. (Table 1), which lies between the doubling times that were previously reported for ES cells cultured in 2i medium in adherent conditions (~13h) and in suspension (30 h ± 5).[61] We conclude that single mES cells can be encapsulated in agarose beads and propagated long-term (68 h) under perfusion conditions, forming monoclonal stem cell spheroids, while remaining undifferentiated.

2.4 Cell Phenotyping in Hydrogel Beads

We evaluated the compatibility of the hydrogel bead format with standard cell biological assays that are performed to determine the state of stem cells in studies aimed at understanding stem cell differentiation and reprogramming, namely immunohistochemistry and RT-qPCR. We encapsulated mES cells in hydrogel beads and cultured them in 2i medium in suspension culture. After 2 days,

beads were fixed and stained for the undifferentiated ES cell markers Oct4 and Nanog.[62-66] After immunostaining, the cells showed a clear nuclear localised signal for both proteins (**Figure 5**A), indicating that the hydrogel bead format did not interfere with the staining procedure. The combination of time-lapse microscopy and subsequent on-chip immunostaining is of particular interest as it allows cell tracking over time followed by staining with defined markers for lineage identification. We tested whether we could perform immunostaining on-chip using a simple set-up that relies on reagents flowing through the trapping array by hydrostatic pressure. To do so, we repeated the same protocol as above. After 2 days of perfusion culture immunostaining of trapped stem cell spheroids was performed by connecting the trapping chip to a syringe with the plunger removed. By positioning the syringe ~10 cm above the trapping chip we were able to perfuse the different reagents by gravity flow. The syringe was sequentially filled with immunostaining reagents. Using this method, cells could be stained on-chip for Sox2, another pluripotency-associated transcription factor [67] (SI and **Figure S5**) and Sox2 positives quantified by automated image analysis (Figure S5C).

Finally, we examined whether agarose-encapsulated cells could be directly analysed using a one step protocol combining reverse transcription and quantitative PCR to quantify mRNA levels from single cells for gene expression profiling. To evaluate the compatibility of the hydrogel format with RT-qPCR, we encapsulated mES cells in hydrogel beads and cultured them in suspension culture for 2 days. To determine whether agarose had an adverse effect on the PCR, we picked single stem cell spheroids located in hydrogel beads, used them directly for RT-qPCR and removed the hydrogel matrix by digestion with agarase prior to RT-qPCR. In addition to stem cell spheroids derived from agarose beads we also analysed cell aggregates of a similar size that were formed under conventional culture conditions without the hydrogel matrix as a control. The presence of the agarose bead as well as the digestion of the agarose matrix with agarase did not affect the pre-amplification protocol or the detection of the mRNA analysed (**Figure 5B**). Both *Pou5f1(*Oct4) and *Nanog* mRNA could be detected at comparable levels to isolated cell aggregates demonstrating the

suitability of this system for extensive cell phenotyping and authenticating cells cultured in beads with behaviour as *bona fide* stem cells. In addition, the possibility of removing the agarose matrix and thereby extracting formed stem cell spheroids from the hydrogel beads allows single-cell analysis of individual colony members.[68, 69]

3. Discussion

The culture conditions and microenvironments can influence the molecular pathways that direct ES cell self-renewal and differentiation: control over these factors is possible in our gel-bead platform, where different media can be administered by feeder pumps and various matrices in addition to agarose could be used. By encapsulating cells with a hydrogel bead, this 3D micro-environment or culture confers better and more realistic growth conditions, e.g. ECM and cell adhesion genes show increased expression in 3D culture over 2D culture. [25, 27] The perfusion of different media in the different channels allowed us to control and monitor the effect of the soluble factors in 2i and N2B27 media over time. Such 3D formats have been applied to stem cells.[26, 27] For encapsulation of single mESCs into hydrogel beads we identified conditions under which the potential impact of each microfluidic step on cells is minimized: for up to four days oil and surfactants seem to have little impact on cell viability for cells cultured in droplets.[8, 10] Afterwards cells become starved of nutrients as medium exchange by perfusion is prohibited by the droplet boundary. Extraction of the gel-bead from the oil phase into an aqueous phase *via* a chemical de-emulsification, (e.g. with perfluorooctanoate, PFO) affects cell viability at the high concentrations of 'demulsifiers' required. Deng *et al.* [70] reported a microfluidic chip for the de-emulsification of alginate beads by inducing droplet merging with an aqueous phase, avoiding the use of surfactant. However, in our case, surfactant stabilisation is required to perform off-chip incubation steps (i.e. on-ice agarose gelification) without droplet merging. Electro-coalescence was previously shown to break emulsions, but required a downstream pipetting step to separate the merged aqueous phase from the

oil phase.[39] The microfluidic chip for the de-emulsification of hydrogel beads presented here overcomes these drawbacks without influencing the viability of mES cells, with each cell exposed to the electric field only for a very short period of time (<100 ms). The design by Fidalgo *et al.*,[40] was modified to suit a wide range of flow rates and enable the merging of denser material with an aqueous stream.

The number of cells that can be cultured and monitored is important, to boost statistical significance and recognize potentially rare events. Different microfluidic single cell traps have been reported,[71-73] some of which are suitable for long-term culture of breast cancer cells, fibroblasts and T-cells.[37, 74, 75] Compared to previous trapping designs for single cells in flow[16, 32, 36], our device has a 2-fold smaller footprint, because a bypassing channel is not required (3.0 *vs* 5.6 traps/mm^2). Single stem cells were cultivated in microdevices, however only up to 672 cells per device, [76, 77] in the absence of a 3D matrix and for shorter (3 hrs) or limited (once per day) time periods.

Few solutions have been devised for the spatial immobilization of hydrogel beads that would allow cell culture in a 3D matrix: an order of magnitude fewer cell-containing beads were trapped in previous work: 28,[78] 70 [33] and 80 [79], respectively, whereas our devices can reach a capacity of 2000 hydrogel beads. In addition, hydrogel beads composed of alginate,[33, 80] agarose[79] or matrigel[81] were used for cell encapsulation and trapping, yet these studies were not extended to experiments probing molecular function (such as the immunostaining and RT-qPCR of encapsulated stem cell colonies shown here) and multiple rather than single cells were encapsulated. Our system paves the way to experiments that rely on precise monitoring of growth starting from single cells under well-defined conditions that emulate cell growth within an environment akin to the extracellular matrix. Cell mobility within bulk 3D matrices makes continuous and long-term (up to 100 hrs) monitoring of single cells and their progenitor cells a particular challenge. Our systems cages cells in a smaller 3D environment, so that clonal colonies are spatially confined. Indeed the 3D framework helps the stem cells to be grown in long-term culture, enabling us to monitor the effect of two different growth media (2i vs N2B27) for 68 hrs to show that the cells in the 2i

medium continue proliferating and expressing the reporter gene (Fig. 4C) beyond the point at which the cells in N2B27 have stopped expressing GFP (i.e. 30 hrs, Fig 4D). For future applications, improvements to allow faster automated image processing (currently limited by the amount of the data recorded) may enable the high-throughput evaluation of the cell cluster or spheroid development, and also the impact of drugs or specific growth factors on clonal populations forming such structures. The four channels of our chip can be used to simultaneously study different parameters such as the influence of different soluble compounds on cell behaviour. The physical microenvironment (e.g. external mechanical forces, matrix mechanics and topographical features) have been shown to affect stem cell differentiation, renewal and proliferation significantly[82-84] and can be further explored with this platform.

4. Conclusion

In this work, we present a modular workflow that will facilitate studying real-time growth kinetics of clonal stem cell colonies as a function of the extracellular 3D microenvironment and of added factors in solution. The heterogeneity of cell populations, as well as the substantial influence of the extracellular matrix on cell behavior, creates the need for an experimental platform that enables the culture and study of colonies derived from single cells in a defined 3D microenvironment. In particular, we established two microfluidic building blocks for the gentle on-chip de-emulsification of droplets containing hydrogel beads and for the spatial immobilization of hydrogel beads for subsequent single cell analysis in long-term perfusion culture, e.g. by time-lapsed microscopy. By evaluating the hydrogel format for the cultivation of mES cells and establishing low melting agarose as an inert scaffold for studying stem cell properties the compatibility of the hydrogel format with downstream molecular techniques was established: namely immunohistochemistry, high-resolution time-lapse confocal microscopy and RT-qPCR. The microfluidic modules and the validation of the hydrogel bead format will pave the way for fast automatic workflows preserving cell viability, while setting the scene for independently addressing the effect of chemical and

mechanical cues on self-renewal and differentiation of mES cells in 3D microenvironments. As each individual clone remains isolated in a bead and a large number of beads can be imaged in parallel, this system will allow the emergence of rare cell populations and the dynamics of differentiation to be examined.[90, 92] The biological impact of experiments carried out in the workflow described above will be boosted by (i) the mild encapsulation, extraction and trapping procedure; (ii) automation that increases ease of handling, but also ensures uniformity of processing steps and cell environment; (iii) the ability to follow monoclonal colonies derived from single cells rather than from heterogeneous populations; (iv) interfacing with imaging techniques such as time-lapsed microscopy that can resolve 3D colony growth for continuous long-term single-cell monitoring of cell morphology and division (e.g. by confocal microscopy). These are particularly important not only for stem cell research[85-87] and clonal lineage tracing,[35] but also for cell-based studies in oncology,[88] developmental biology[89, 90] and immunology,[91] where culture and testing of large numbers of single cells in parallel and at low cost through small sample volumes is desired. Here such culture can be carried out under highly controlled physiological conditions, where 'stemness' of mES cells can be controlled (i.e. in a matrix environment and under well-defined biochemical conditions), that will make this live-cell array a useful tool to study extrinsic regulation with clonal resolution.

5. Experimental Section

Chip Fabrication: Polydimethylsiloxane (PDMS; Sylgard® 184 silicone elastomer kit, Dow Corning) chips were fabricated using soft lithography (see SI for designs and detailed procedures; design files will be deposited at http://openwetware.org/wiki/DropBase). Master molds were fabricated using SU8-2025 (Microchem) as negative photoresist and film masks designed with AutoCAD 2013 (Autodesk). The master molds were coated with PFOTS (Sigma Aldrich) by chemical vapour deposition. PDMS chips were either bound to a glass slide or to a thin PDMS layer using oxygen plasma treatment (FEMTO, Diener electronic).

Cell Culture: Two different mES cell lines were used in this study: E14Tg2a.IV [50] and (RGd2) expressing destabilized GFP (half life: approximately 2h) under the promotor of Rex1 (gene name *Zfp42*).[53, 93, 94] Both cell lines were cultivated in 2i-medium (where mES cells maintain pluripotency under the dual inhibition of Mek/Erk and GSK3 pathways), containing 1 µM PD0325901, 3 µM CH99021 and 1% streptomycin/penicillin in N2B27.[50] Cells were dissociated with Accutase (PAA), followed by neutralisation with DMEM/F12/0.1% BSA (Life Technologies/Gibco), centrifugation and re-suspension in 2i for re-plating.

Cell Encapsulation: mES cells were encapsulated in hydrogel beads as described previously[95] using a microfluidic chip with a flow focussing geometry.[30] The microfluidic chip had one inlet for an aqueous phase (6,000 cells/µl in PBS or 2i-medium medium containing 1.5% (w/v) SeaPrep™ agarose (Lonza) that was kept liquid in solution (at 37 °C) and a second inlet for the oil/carrier phase (3M™ Novec™ Engineered fluid (HFE 7500) (Fluorochem) containing 1% (w/w) AZC2 [96]). The microfluidic chip was coated with 1% (v/v) PFOTS in HFE-7500 directly after the plasma bonding (see SI). For cell encapsulation, the cell suspension was transferred into a 1 ml syringe that was maintained at 37 °C (to keep the agarose solution liquid) using a 12 V heating foil (Conrad Electronics) operated by a custom-made temperature controller (Figure S6). The flow rates for droplet generation at 291 ± 11 Hz were: carrier phase: 30 µl/min, aqueous phase: 6 µl/min.[97, 98] Agarose droplets containing cells were collected and incubated on ice (~5 min) to allow gelification into a bead format. Immediately, de-emulsification was performed either using 1H,1H,2H,2H-perfluorooctanol (PFO) (97%, Alfa Aesar) or on-chip.

On-Chip De-emulsification: For the on-chip de-emulsification of the encapsulated hydrogel beads a microfluidic design with two intersecting channels was used to extract the hydrogel beads from the oil phase into an aqueous phase. The design for the microfluidic chip is shown in Figure S1C and D.

The microfluidic chip has three inlets: one for the aqueous phase (PBS or cell culture medium), one for the oil phase containing hydrogel microdroplets and one for a sheath fluid (HFE-7500 and 1% (w/w) AZC2) that was used for hydrodynamic focusing and spacing of incoming droplets.[8] Two electrodes made of low-melting indium alloys (51 IN, 32.5 BI, 16.5 SN; Indium Corporation of America) are located at either side of the intersecting channels. These electrodes were used for inducing electro-coalescence between droplets and the aqueous phase by applying an electric AC field (Model 601C, TREK). To increase the stability of the oil/water interface, the channel for the aqueous phase was coated with acrylic acid (procedure based on [42] and the channel for the oil phase was coated with PFOTS (see SI).

Spatial Immobilization of Hydrogel Beads: De-emulsified SeaPrep™ agarose beads (1.5% (w/v) in PBS (Life Technologies)) were diluted to obtain a hydrogel bead concentration of 50 beads/µl. The trapping chip was perfused with a constant volume (20 µl) of the bead solution at various flow rates using a syringe pump (Nemesys Low pressure, Cetoni). The maximum flow of 150µl//min used in our system suggest that shear stress does not have an effect on cells, which, in addition, are protected by the surrounding hydrogel. [97, 98]

Perfusion Culture and Confocal Time-Lapsed Microscopy: MES cells (GFP expression coupled to promotor of Rex-1)[93, 94] were encapsulated in 1.5% (w/v) SeaPrep™ agarose beads, de-emulsified and diluted to a concentration of 50 beads/µl. The bead solution was mixed to resuspend the beads, and immediately syphoned up into tubing for re-injection into to the trapping chip to minimize loss of beads. Hydrogel beads were transferred into the trapping chip using either a syringe pump or by manual operation of the syringe. After immobilization of hydrogel beads, the trapping chip was connected to a different syringe to perfuse either N2B27 or 2i-medium and cells were cultivated (68 h, perfusion at 2µl/min flow rate). Time-lapsed confocal microscopy (Leica SP5 TCS, Leica

Microsystems) was performed in an incubation chamber (37°C, 7% CO_2). Images were analysed with the open source software ImageJ (www.imagej.net) (see SI for details).

Immunostaining of Hydrogel Beads in Bulk: Hydrogel beads containing clonal colonies were fixed with 4% paraformaldehyde (Sigma) (10 min, RT), before washing twice with PBS. Cell permeabilization and blocking was performed by incubating hydrogel beads (3 h, RT) with 3% (v/v) Donkey serum (Sigma) in PBS containing 0.03% (v/v) TritonX (Sigma) (block buffer). The beads were then incubated in block buffer containing primary antibodies (4 °C, overnight). Hydrogel beads were washed three times (10 min in PBS containing 0.03% (v/v) TritonX) to remove unspecific binding before incubating with secondary antibodies and 1 μg/ml DAPI (Life Technologies) in block buffer (3 h, RT, in the dark). Finally, beads were washed three times (10 min in PBS containing 0.03% (v/v) Triton X). For mounting, beads were passed though solutions containing 25%, 50% and 75% of VECTASHIELD mounting medium (Vector Laboratories) in PBS, before mounting on glass slides. Confocal imaging (Leica SP5 TCS, Leica microsystems) was done using 305 nm, 488 nm and 545 nm lasers. Primary antibodies used were Oct4 (1:400, Santa Cruz) and Nanog (1:300, eBioscience). Secondary antibodies used were Donkey anti-Mouse Alexa Fluor 488 and Donkey anti-Rat Alexa Fluor 555 at a 1:1000 dilution (Life Techologies).

Immunostaining of Cells in Immobilized Hydrogel Beads: For immunostaining, the trapping chip inlets were connected to an open syringe (plunger was removed) where each solution was sequentially flowed through (order and timings as described above). The syringe was positioned vertically 10 cm above the trapping chip to facilitate flow by hydrostatic pressure. On the last wash, the solution was changed to PBS and the inlets and outlets were blocked. The chip was then imaged using confocal microscopy. The primary antibody was against Sox2 (1:200, eBioscience) and the secondary antibody was the donkey anti-Rat Alexa 488 (Life Technologies) at 1:1000 dilution.

Automatic quantification was performed using the MicroArray Profile plug-in for ImageJ (http://www.optinav.com/MicroArray_Profile.htm). Beads were scored positive when the following criteria were met: max. intensity = 255, standard deviation >25.

RT-qPCR: Beads or cell aggregates were transferred by a mouth pipette to 8-well strips containing CellsDirect One-Step RT-qPCR reagents following manufacturer's instructions (Ambion, Invitrogen) for cDNA synthesis and pre-amplification. The final product was diluted 100 times in nuclease free water and stored at -20°C. qPCR was carried out using Fast SYBR Green Master Mix (Life Technologies).

Supporting Information

Supporting Information is available from the Wiley Online Library or from the author.

Acknowledgements

We thank Sakonwan Kuhaudomlarp for help with preliminary experiments and T.N. Kohler for helpful advice and comments on the manuscript. This research described was funded by the Wellcome Trust (WT108438/C/15/Z), the Engineering and Physical Sciences Research Council (EPSRC), the EU via its Horizon2020 programme and the Medical Research Council (MRC). The Cambridge Stem Cell Institute receives core funding from the Wellcome Trust and the MRC. AS is an MRC Professor; KC and FH are ERC Investigators. HKB held fellowships by the Studienstiftung des deutschen Volkes and the German Academic Exchange Service (DAAD).

Received: (will be filled in by the editorial staff)
Revised: (will be filled in by the editorial staff)
Published online: (will be filled in by the editorial staff)

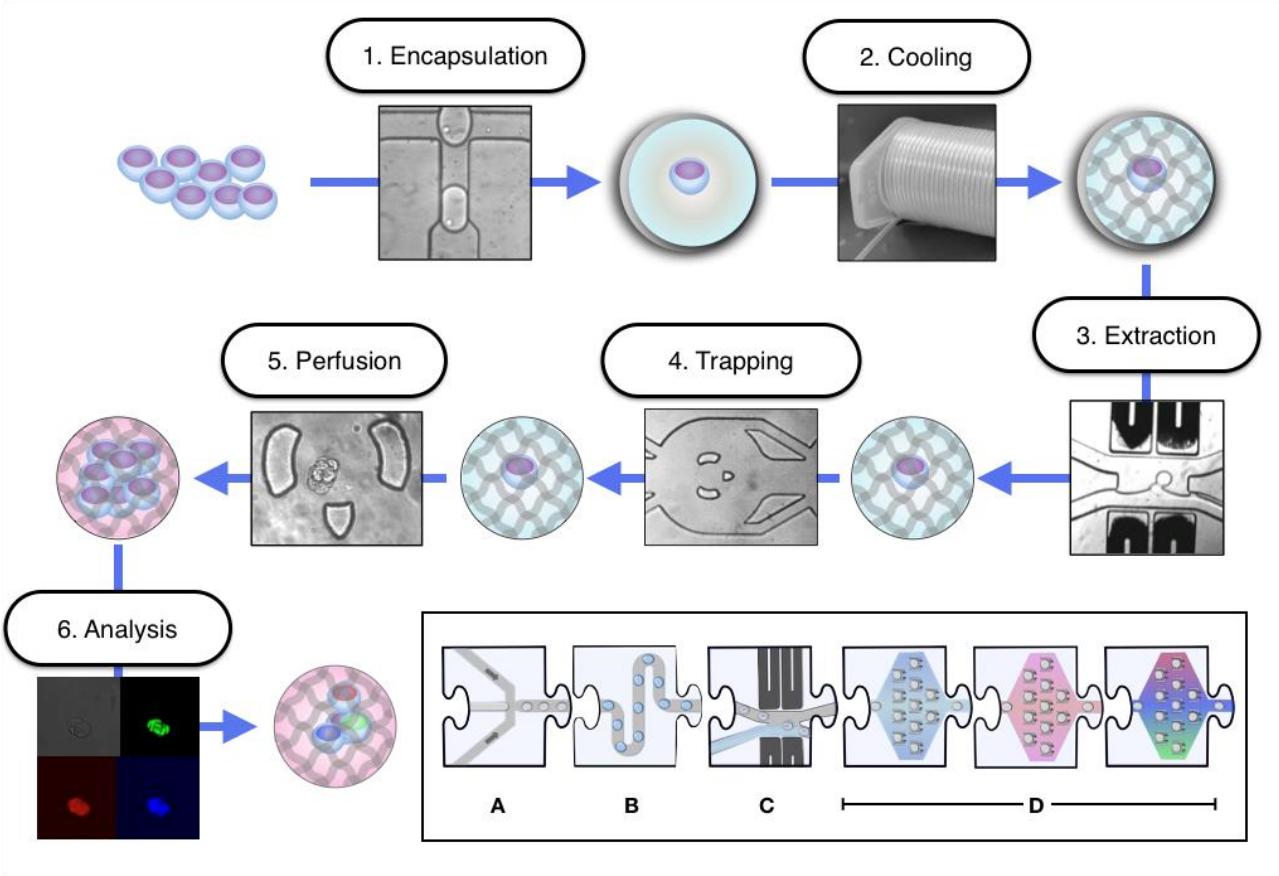

Figure 1. The workflow established in this work for cultivating clonal embryonic stem cell colonies. The steps include: (1) Encapsulation of single cells into hydrogel droplets (at 291 ± 11 Hz) using droplet-based microfluidics (A), (2) cooling and hydrogel formation (symbolised by grey pattern) within microdroplets by incubation in cooled tubing (B); (3) On-chip de-emulsification of droplets containing single cells encapsulated in hydrogel beads using electro-coalescence (C), performed in line after encapsulation; (4) Spatial immobilization of hydrogel beads, (5) long-term perfusion culture and time-lapsed microscopy and (6) analysis (e.g. fluorescent read-out, immunostaining, RT-qPCR) in a trapping device (D).

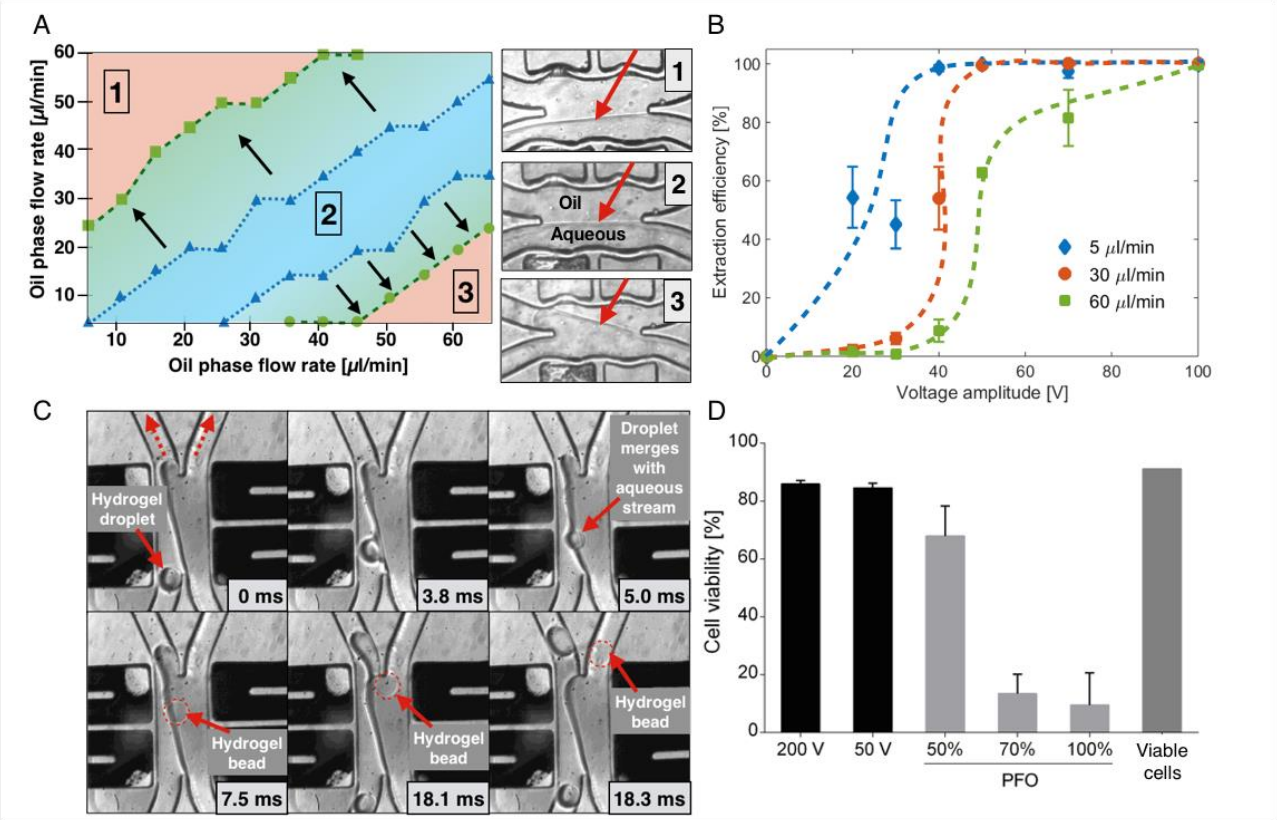

Figure 2. On-chip de-emulsification of microdroplets containing Poisson-distributed cells encapsulated in hydrogel beads. A) Influence of the differential channel coating on the interface stability. Coating one channel with PAA and the other channel with PFOTS increases the operational window (number of stable flow rate pairs, from blue section to green). (1) Leakage of the oil phase into the aqueous phase channel. (2) Stable interface between the two phases. (3) Leakage of the water phase into the oil channel. Flow rates producing a stable interface are shown for a chip before (blue) and after coating (green). The red area represents flow rates at which leakage could be observed. B) Influence of the voltage amplitude on the extraction efficiency at different flow rates of the sheath fluid. Measurements were performed in triplicates. Error bars represent standard error. Frequency of applied AC field: 1 kHz. See the SI (Fig. S7) for a correlation of residence time of droplets passing across the oil-water interface as a function of sheath fluid flow rate. C) Time frame snapshots of the de-emulsification process. Dotted red arrows represent flow direction of the aqueous phase (left channel) and the carrier phase (right channel). D) Cell viability of mES cells after de-emulsification. Compared to PFO de-emulsification, de-emulsification using electro-coalescence achieves a 9-fold higher viability. Three technical replicates were performed. Error bars represent the standard deviations.

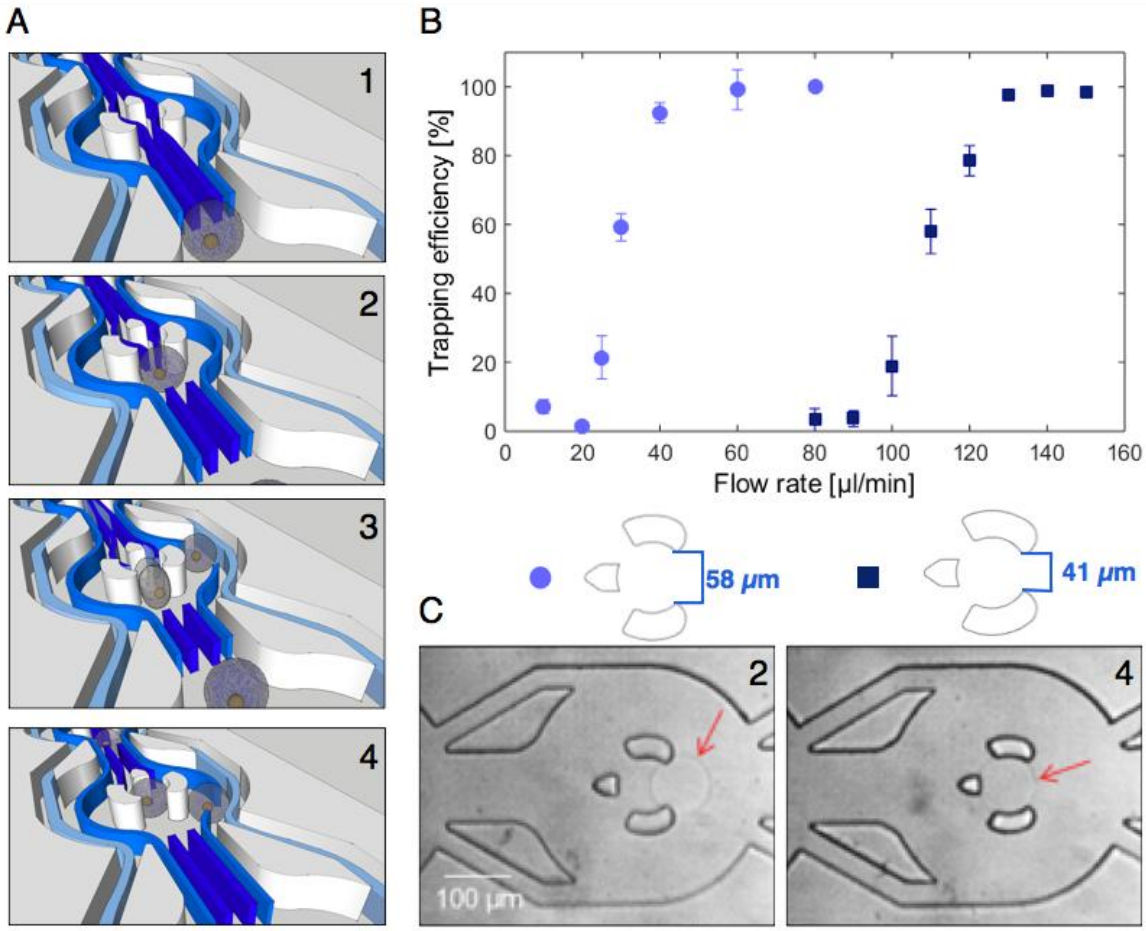

Figure 3. Relationship between flow rate and trapping efficiency and illustration of the trapping of hydrogel beads. (A) Illustration of the trapping mechanism in a series of time-resolved sketches. Faster flow is observed in the middle of the channel (dark blue) and slower flow by the channel walls (light blue). The hydrogel beads follow the strongest flow towards the center of the channel (1) until the bead hits the edge of the trapping compartment (2), it is then hydrodynamically pushed into the trapping device and squeezed to enter the trap through an opening of either 41 µm or 58 µm (3). Once a bead is trapped (4) the other beads flow until they are pushed through the next available trap. (B) Influence of the flow rate as well as trap opening (41µm or 58 µm) on the trapping efficiency. Measurements were performed in triplicates. Error bars represent standard deviation. (C) Brightfield images of beads lodged in front of the trap (2) or when fully trapped (4), respectively.

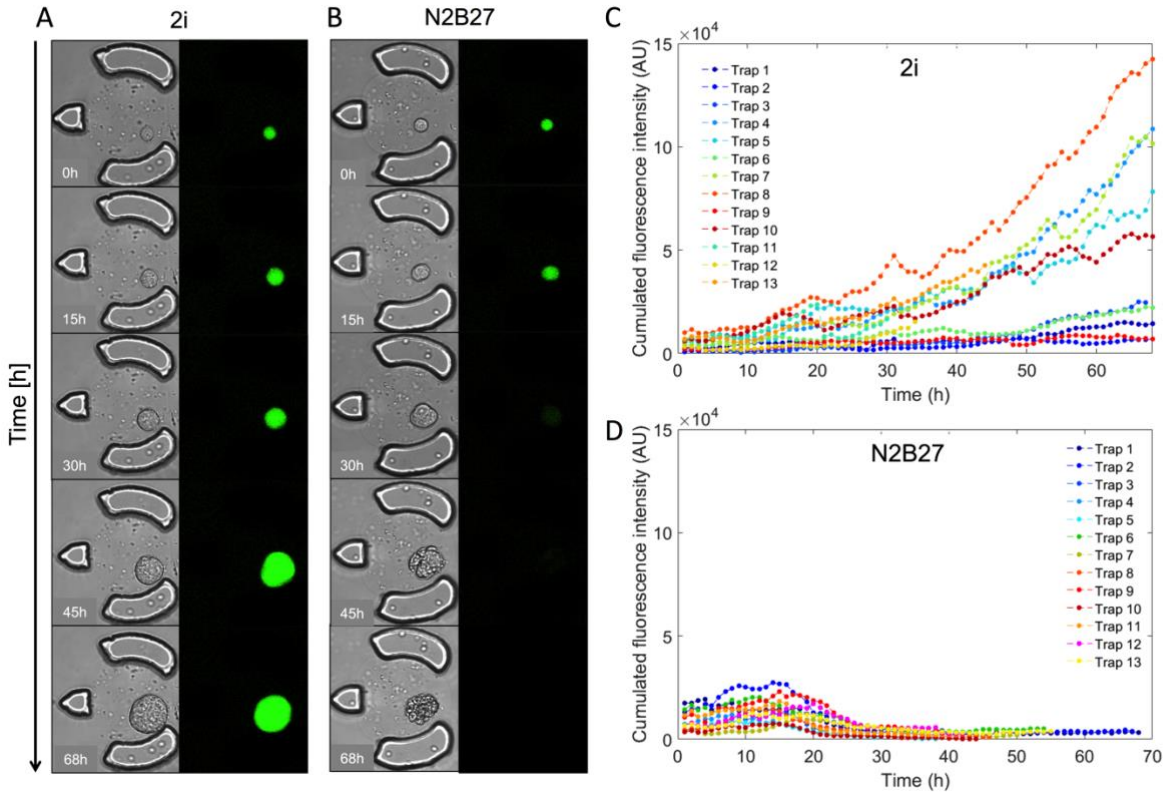

Figure 4. Perfusion culture and time-lapse confocal microscopy of mES cells encapsulated in agarose beads under two growth conditions over 68 hours. **(A&B)** Time-lapse bright field and fluorescence confocal microscopy of immobilized single mES cell (Rex1-GFPd2) encapsulated in a trapped hydrogel bead that forms a monoclonal stem cell spheroid after 68h, when perfused with 2i (A) or N2B27 (B). GFP expression marking pluripotency (under the Rex-1 promoter) is switched off for cells perfused with the base medium N2B27 after 15 hrs. **(C&D)** Time-courses of the fluorescence intensity of mES cell clonal colonies grown in 2i (C) or N2B27 (D). Each line represents the calculated pixel intensity for one monoclonal colony, 13 representative colonies in 2i (B) or N2B27 (C). The cumulated fluorescence intensity decreased after 20 to 25 hours for cells cultivated in N2B27, while it continued to increase for cells grown in 2i. This indicates that the mES cells exit pluripotency when the culture medium is switched from 2i to N2B27. Of the 13 gel beads monitored in 2i medium, five beads (traps 1-3, 6 and 9) showed slower cell growth, cell colonies in traps 11-13 escaped the gel bead (C, video S4 and correlating traps in video S6). *Cumulated Fluorescence:* intensity was calculated by adding the pixel intensity of the z-stacks gained with the confocal microscope**.** The z-projection was then used to calculate the integrated pixel density.

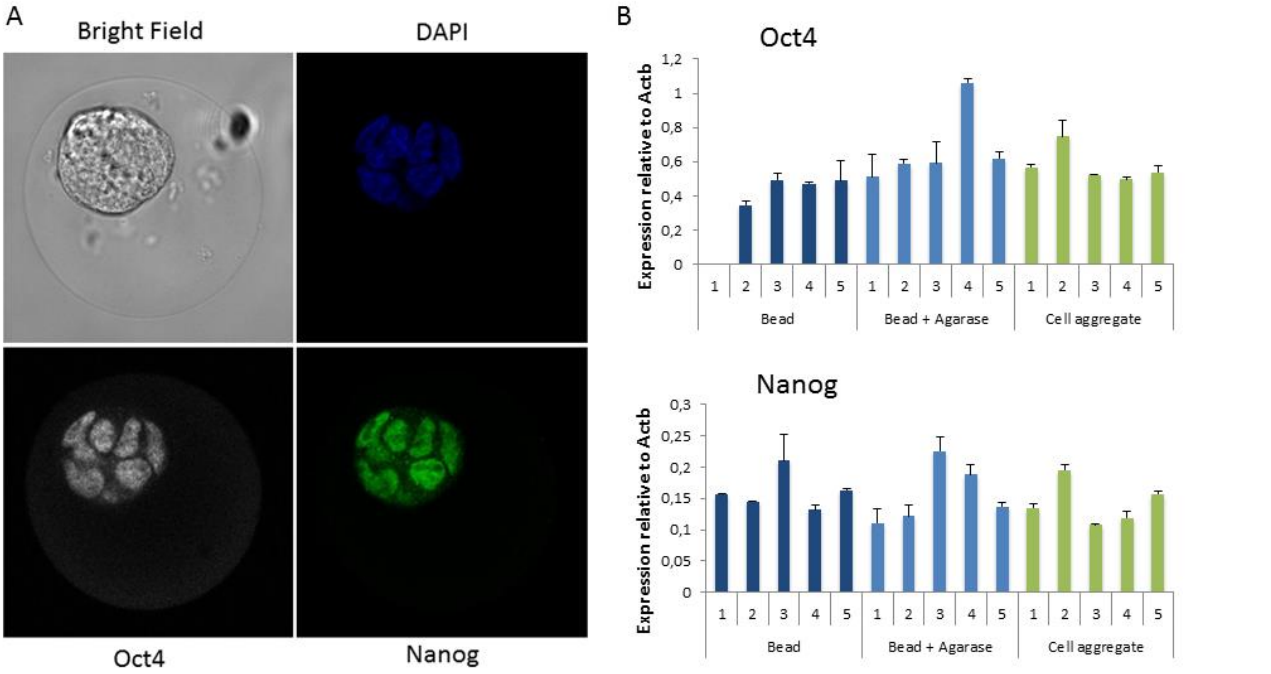

Figure 5. Immunostaining and RT-qPCR of encapsulated stem cell colonies grown (2 days) from Poisson distributed single cells. (A) Mouse embryonic stem cells were stained for expression of Oct4 and Nanog. Nuclei were stained with DAPI. (B) RT-qPCR of agarose beads containing cell colonies. In total five beads/cell colonies were analyzed for each condition. Beta actin (Actb) was used as endogenous control for relative gene expression quantification. The experiment was performed with three technical replicates. Error bars represent the standard deviation.

Table 1. Growth rates of monoclonal stem cell colonies located at 13 different trap positions. The growth rate μ was determined by fitting the cumulated fluorescence data with a single-term exponential model ($f(x) = a\,e^{\mu t}$) using the software Matlab. The doubling time T_d was calculated as $T_d = \ln(2)/\mu$. The given error of the growth rate represents the 95% confidence interval. Corresponding growth curves are shown in Figure 4 and in Video S6.

Trap	Growth Rate μ (h^{-1})	Doubling Time T_d (h)
1	0.028 ± 0.003	24.6
2	0.024 ± 0.003	29.0
3	0.049 ± 0.003	14.2
4	0.046 ± 0.001	14.9
5	0.033 ± 0.002	20.9
6	0.025 ± 0.002	28.0
7	0.045 ± 0.002	15.3
8	0.038 ± 0.001	18.1
9	0.016 ± 0.003	43.9
10	0.029 ± 0.002	23.6
11	0.017 ± 0.017	40.9
12	0.086 ± 0.013	8.0
13	0.050 ± 0.002	14.9

Kleine-Brüggeney *et. al.* grow mouse embryonic stem cell clones in microfluidic microcompartments from single cells. Stem cells proliferate in agarose beads that mimic a natural 3D environment, form clonal colonies and can be interrogated by optical and molecular analysis.

Keyword: Single stem cell analysis in hydrogels

Hans Kleine-Brüggeney, Liisa D. Van Vliet, Carla Mulas, Fabrice Gielen, Chibeza C. Agley, José C.R. Silva, Austin Smith, Kevin Chalut and Florian Hollfelder*

Table-of-contents Figure

Long-term perfusion culture of monoclonal embryonic stem cells in 3D hydrogel beads for continuous optical analysis

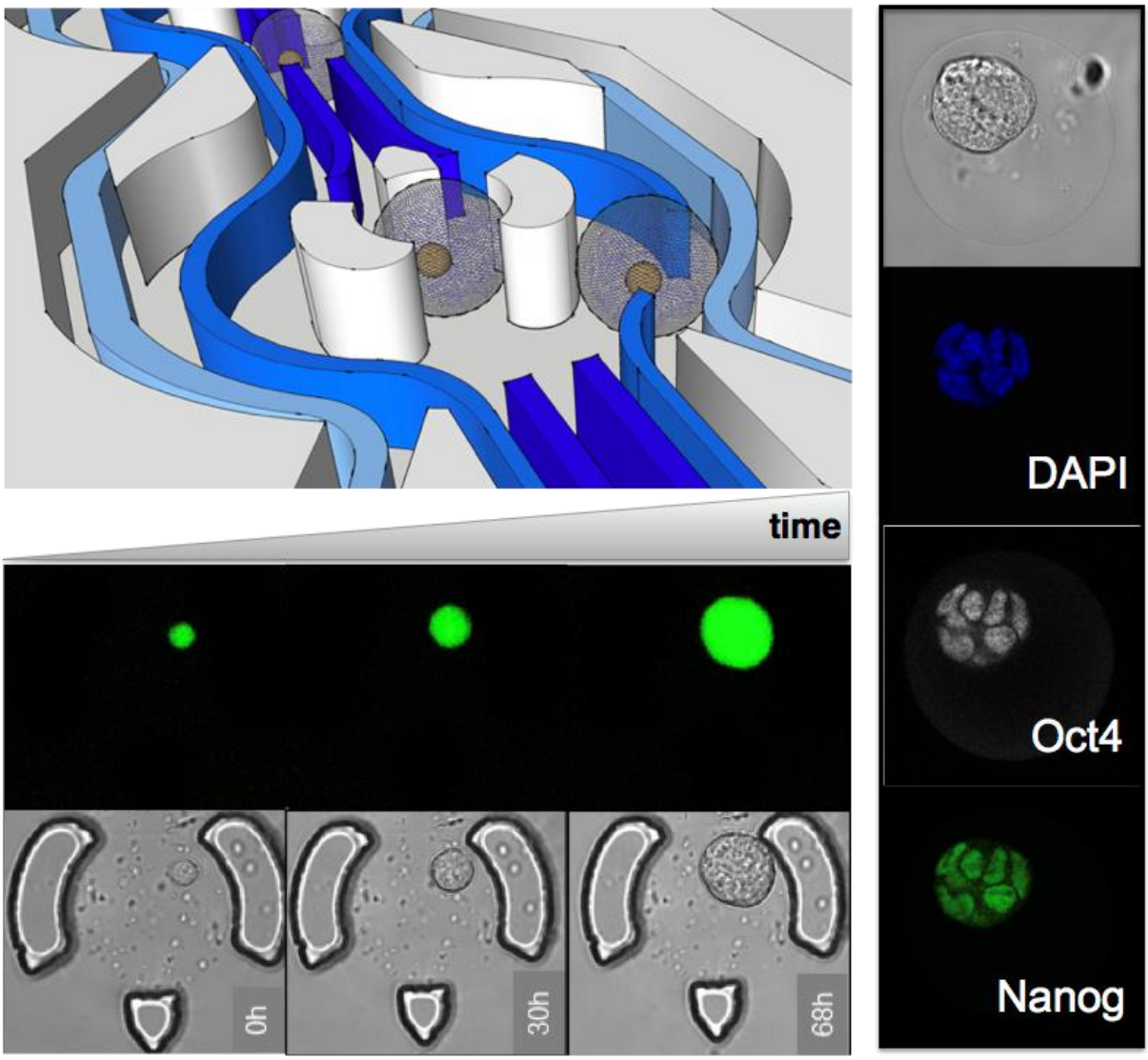

References

1. Theberge, A. B.; Courtois, F.; Schaerli, Y.; Fischlechner, M.; Abell, C.; Hollfelder, F.; Huck, W. T., *Angew Chem Int Ed Engl* **2010,** *49* (34), 5846-68. DOI 10.1002/anie.200906653.
2. Huebner, A.; Sharma, S.; Srisa-Art, M.; Hollfelder, F.; Edel, J. B.; Demello, A. J., *Lab on a chip* **2008,** *8* (8), 1244-54. DOI 10.1039/b806405a.
3. Schaerli, Y.; Hollfelder, F., *Mol Biosyst* **2009,** *5* (12), 1392-404. DOI 10.1039/b907578j.
4. Huebner, A.; Srisa-Art, M.; Holt, D.; Abell, C.; Hollfelder, F.; deMello, A. J.; Edel, J. B., *Chemical Communications* **2007,** (12), 1218-20. DOI 10.1039/b618570c.
5. Shim, J. U.; Olguin, L. F.; Whyte, G.; Scott, D.; Babtie, A.; Abell, C.; Huck, W. T.; Hollfelder, F., *J Am Chem Soc* **2009,** *131* (42), 15251-6. DOI 10.1021/ja904823z.
6. Huebner, A.; Olguin, L. F.; Bratton, D.; Whyte, G.; Huck, W. T.; de Mello, A. J.; Edel, J. B.; Abell, C.; Hollfelder, F., *Analytical chemistry* **2008,** *80* (10), 3890-6. DOI 10.1021/ac800338z.
7. Hufnagel, H.; Huebner, A.; Gulch, C.; Guse, K.; Abell, C.; Hollfelder, F., *Lab Chip* **2009,** *9* (11), 1576-82. DOI 10.1039/b821695a.
8. Clausell-Tormos, J.; Lieber, D.; Baret, J. C.; El-Harrak, A.; Miller, O. J.; Frenz, L.; Blouwolff, J.; Humphry, K. J.; Koster, S.; Duan, H.; Holtze, C.; Weitz, D. A.; Griffiths, A. D.; Merten, C. A., *Chem Biol* **2008,** *15* (5), 427-37. DOI 10.1016/j.chembiol.2008.04.004.
9. Mazutis, L.; Gilbert, J.; Ung, W. L.; Weitz, D. A.; Griffiths, A. D.; Heyman, J. A., *Nat Protoc* **2013,** *8* (5), 870-91. DOI 10.1038/nprot.2013.046.
10. Brouzes, E.; Medkova, M.; Savenelli, N.; Marran, D.; Twardowski, M.; Hutchison, J. B.; Rothberg, J. M.; Link, D. R.; Perrimon, N.; Samuels, M. L., *Proc Natl Acad Sci U S A* **2009,** *106* (34), 14195-200. DOI 10.1073/pnas.0903542106.
11. Utech, S.; Prodanovic, R.; Mao, A. S.; Ostafe, R.; Mooney, D. J.; Weitz, D. A., *Adv Healthc Mater* **2015,** *4* (11), 1628-33. DOI 10.1002/adhm.201500021.
12. Velasco, D.; Tumarkin, E.; Kumacheva, E., *Small* **2012,** *8* (11), 1633-42. DOI 10.1002/smll.201102464.
13. Fischlechner, M.; Schaerli, Y.; Mohamed, M. F.; Patil, S.; Abell, C.; Hollfelder, F., *Nat Chem* **2014,** *6* (9), 791-6. DOI 10.1038/nchem.1996.
14. Gasperini, L.; Mano, J. F.; Reis, R. L., *J R Soc Interface* **2014,** *11* (100), 20140817. DOI 10.1098/rsif.2014.0817.
15. van Duinen, V.; Trietsch, S. J.; Joore, J.; Vulto, P.; Hankemeier, T., *Curr Op Biotechnol* **2015,** *35*, 118-126. DOI 10.1016/j.copbio.2015.05.002.
16. Tan, W. H.; Takeuchi, S., *Lab Chip* **2008,** *8* (2), 259-66. DOI 10.1039/b714573j.
17. Tsuda, Y.; Morimoto, Y.; Takeuchi, S., *Langmuir* **2010,** *26* (4), 2645-2649. DOI 10.1021/la002827y.
18. Zhu, Z.; Yang, C. J., *Acc Chem Res* **2017,** *50* (1), 22-31. DOI 10.1021/acs.accounts.6b00370.
19. Walling, M. A.; Shepard, J. R., *Chem Soc Rev* **2011,** *40* (7), 4049-76. DOI 10.1039/c0cs00212g.
20. Hoppe, P. S.; Coutu, D. L.; Schroeder, T., *Nat Cell Biol* **2014,** *16* (10), 919-27. DOI 10.1038/ncb3042.
21. Mao, A. S.; Shin, J. W.; Utech, S.; Wang, H.; Uzun, O.; Li, W.; Cooper, M.; Hu, Y.; Zhang, L.; Weitz, D. A.; Mooney, D. J., *Nat Mater* **2017,** *16* (2), 236-243. DOI 10.1038/nmat4781.
22. Toh, Y. C.; Xing, J.; Yu, H., *Biomaterials* **2015,** *50*, 87-97. DOI 10.1016/j.biomaterials.2015.01.019.
23. Roch, A.; Giger, S.; Girotra, M.; Campos, V.; Vannini, N.; Naveiras, O.; Gobaa, S.; Lutolf, M. P., *Nat Comm* **2017,** *8* (1), 221. DOI 10.1038/s41467-017-00291-3.
24. Tabata, Y.; Lutolf, M. P., *Sci Rep* **2017,** *7*, 44711. DOI 10.1038/srep44711.
25. Luca, A. C.; Mersch, S.; Deenen, R.; Schmidt, S.; Messner, I.; Schafer, K. L.; Baldus, S. E.; Huckenbeck, W.; Piekorz, R. P.; Knoefel, W. T.; Krieg, A.; Stoecklein, N. H., *PloS One* **2013,** *8* (3), e59689. DOI 10.1371/journal.pone.0059689.

26. Wei, J.; Han, J.; Zhao, Y.; Cui, Y.; Wang, B.; Xiao, Z.; Chen, B.; Dai, J., *Biomaterials* **2014,** *35* (27), 7724-33. DOI 10.1016/j.biomaterials.2014.05.060.
27. Liu, H.; Lin, J.; Roy, K., *Biomaterials* **2006,** *27* (36), 5978-89. DOI 10.1016/j.biomaterials.2006.05.053.
28. Lutolf, M. P.; Gilbert, P. M.; Blau, H. M., *Nature* **2009,** *462* (7272), 433-41. DOI 10.1038/nature08602.
29. Caiazzo, M.; Okawa, Y.; Ranga, A.; Piersigilli, A.; Tabata, Y.; Lutolf, M. P., *Nat Materials* **2016,** *15* (2), 344-52. DOI 10.1038/nmat4536.
30. Anna, S. L.; Bontoux, N.; Stone, H. A., *Appl Phys Lett* **2003,** *82* (3), 364-366. DOI 10.1063/1.1537519.
31. Sart, S.; Tomasi, R. F.; Amselem, G.; Baroud, C. N., *Nature communications* **2017,** *8* (1), 469. DOI 10.1038/s41467-017-00475-x.
32. Tonooka, T.; Teshima, T.; Takeuchi, S., *Microfluidics and Nanofluidics* **2013,** *14* (6), 1039-1048. DOI 10.1007/s10404-012-1111-7.
33. Kim, C.; Bang, J. H.; Kim, Y. E.; Lee, J. H.; Kang, J. Y., *Sensors and Actuators B: Chemical* **2012,** *166-167*, 859-869. DOI 10.1016/j.snb.2012.02.008.
34. Schroeder, T., *Nat Meth* **2011,** *8* (4 Suppl), S30-5. DOI 10.1038/nmeth.1577.
35. Etzrodt, M.; Endele, M.; Schroeder, T., *Cell Stem Cell* **2014,** *15* (5), 546-58. DOI 10.1016/j.stem.2014.10.015.
36. Teshima, T.; Ishihara, H.; Iwai, K.; Adachi, A.; Takeuchi, S., *Lab Chip* **2010,** *10* (18), 2443-8. DOI 10.1039/c004986g.
37. Kobel, S.; Valero, A.; Latt, J.; Renaud, P.; Lutolf, M., *Lab Chip* **2010,** *10* (7), 857-63. DOI 10.1039/b918055a.
38. Kim, H.; Lee, S.; Kim, J., *Microfluidics and Nanofluidics* **2012,** *13* (5), 835-844. DOI 10.1007/s10404-012-1006-7.
39. Chokkalingam, V.; Ma, Y.; Thiele, J.; Schalk, W.; Tel, J.; Huck, W. T., *Lab Chip* **2014,** *14* (14), 2398-402. DOI 10.1039/c4lc00365a.
40. Fidalgo, L. M.; Whyte, G.; Bratton, D.; Kaminski, C. F.; Abell, C.; Huck, W. T., *Angew Chem Int Ed Engl* **2008,** *47* (11), 2042-5. DOI 10.1002/anie.200704903.
41. Fallah-Araghi, A.; Baret, J. C.; Ryckelynck, M.; Griffiths, A. D., *Lab Chip* **2012,** *12* (5), 882-91. DOI 10.1039/c2lc21035e.
42. Schneider, M. H.; Willaime, H.; Tran, Y.; Rezgui, F.; Tabeling, P., *Anal Chem* **2010,** *82* (21), 8848-55. DOI 10.1021/ac101345m.
43. Doms, M.; Feindt, H.; Kuipers, W. J.; Shewtanasoontorn, D.; Matar, A. S.; Brinkhues, S.; Welton, R. H.; Mueller, J., *Journal of Micromechanics and Microengineering* **2008,** *18* (5), 055030. DOI 10.1088/0960-1317/18/5/055030.
44. Niu, X.; Gielen, F.; deMello, A. J.; Edel, J. B., *Anal Chem* **2009,** *81* (17), 7321-5. DOI 10.1021/ac901188n.
45. Kim, C.; Lee, K. S.; Kim, Y. E.; Lee, K. J.; Lee, S. H.; Kim, T. S.; Kang, J. Y., *Lab Chip* **2009,** *9* (9), 1294-1297. DOI 10.1039/b819044e.
46. Hazenbiller, O.; Duncan, N. A.; Krawetz, R. J., *BMC Cell Biol* **2017,** *18* (1), 32. DOI 10.1186/s12860-017-0148-6.
47. Alexandrova, S.; Kalkan, T.; Humphreys, P.; Riddell, A.; Scognamiglio, R.; Trumpp, A.; Nichols, J., *Development* **2016,** *143* (1), 24-34. DOI 10.1242/dev.124602.
48. Megyola, C. M.; Gao, Y.; Teixeira, A. M.; Cheng, J.; Heydari, K.; Cheng, E. C.; Nottoli, T.; Krause, D. S.; Lu, J.; Guo, S., *Stem Cells* **2013,** *31* (5), 895-905. DOI 10.1002/stem.1323.
49. Hilsenbeck, O.; Schwarzfischer, M.; Skylaki, S.; Schauberger, B.; Hoppe, P. S.; Loeffler, D.; Kokkaliaris, K. D.; Hastreiter, S.; Skylaki, E.; Filipczyk, A.; Strasser, M.; Buggenthin, F.; Feigelman, J. S.; Krumsiek, J.; van den Berg, A. J.; Endele, M.; Etzrodt, M.; Marr, C.; Theis, F. J.; Schroeder, T., *Nat Biotechnol* **2016,** *34* (7), 703-6. DOI 10.1038/nbt.3626.

50. Ying, Q. L.; Wray, J.; Nichols, J.; Batlle-Morera, L.; Doble, B.; Woodgett, J.; Cohen, P.; Smith, A., *Nature* **2008,** *453* (7194), 519-23. DOI 10.1038/nature06968.
51. Silva, J.; Barrandon, O.; Nichols, J.; Kawaguchi, J.; Theunissen, T. W.; Smith, A., *PLoS Biol* **2008,** *6* (10), e253. DOI 10.1371/journal.pbio.0060253.
52. Marks, H.; Kalkan, T.; Menafra, R.; Denissov, S.; Jones, K.; Hofemeister, H.; Nichols, J.; Kranz, A.; Stewart, A. F.; Smith, A.; Stunnenberg, H. G., *Cell* **2012,** *149* (3), 590-604. DOI 10.1016/j.cell.2012.03.026.
53. Wray, J.; Kalkan, T.; Gomez-Lopez, S.; Eckardt, D.; Cook, A.; Kemler, R.; Smith, A., *Nat Cell Biol* **2011,** *13* (7), 838-45. DOI 10.1038/ncb2267.
54. Kalkan, T.; Smith, A., *Philosophical transactions of the Royal Society of London. Series B, Biol Sci* **2014,** *369* (1657). DOI 10.1098/rstb.2013.0540.
55. Betschinger, J.; Nichols, J.; Dietmann, S.; Corrin, P. D.; Paddison, P. J.; Smith, A., *Cell* **2013,** *153* (2), 335-47. DOI 10.1016/j.cell.2013.03.012.
56. Cho, M.; Cho, T.-J.; Lim, J. M.; Lee, G.; Cho, J., *Molecules Cells* **2013,** *35* (5), 456-461.
57. Vogel, R., *Reproductive Toxicology* **1993,** *7 Suppl 1*, 69-73.
58. Kunath, T.; Saba-El-Leil, M. K.; Almousailleakh, M.; Wray, J.; Meloche, S.; Smith, A., *Development* **2007,** *134* (16), 2895-902. DOI 10.1242/dev.02880.
59. Stavridis, M. P.; Lunn, J. S.; Collins, B. J.; Storey, K. G., *Development* **2007,** *134* (16), 2889-94. DOI 10.1242/dev.02858.
60. Lienemann, P. S.; Rossow, T.; Mao, A. S.; Vallmajo-Martin, Q.; Ehrbar, M.; Mooney, D. J., *Lab Chip* **2017,** *17* (4), 727-737. DOI 10.1039/c6lc01444e.
61. Tamm, C.; Pijuan Galito, S.; Anneren, C., *PloS One* **2013,** *8* (12), e81156. DOI 10.1371/journal.pone.0081156.
62. Nichols, J.; Zevnik, B.; Anastassiadis, K.; Niwa, H.; Klewe-Nebenius, D.; Chambers, I.; Scholer, H.; Smith, A., *Cell* **1998,** *95* (3), 379-91.
63. Niwa, H.; Miyazaki, J.; Smith, A. G., *Nat Gen* **2000,** *24* (4), 372-6. DOI 10.1038/74199.
64. Chambers, I.; Colby, D.; Robertson, M.; Nichols, J.; Lee, S.; Tweedie, S.; Smith, A., *Cell* **2003,** *113* (5), 643-55.
65. Mitsui, K.; Tokuzawa, Y.; Itoh, H.; Segawa, K.; Murakami, M.; Takahashi, K.; Maruyama, M.; Maeda, M.; Yamanaka, S., *Cell* **2003,** *113* (5), 631-42.
66. Chambers, I.; Silva, J.; Colby, D.; Nichols, J.; Nijmeijer, B.; Robertson, M.; Vrana, J.; Jones, K.; Grotewold, L.; Smith, A., *Nature* **2007,** *450* (7173), 1230-4. DOI 10.1038/nature06403.
67. Masui, S.; Nakatake, Y.; Toyooka, Y.; Shimosato, D.; Yagi, R.; Takahashi, K.; Okochi, H.; Okuda, A.; Matoba, R.; Sharov, A. A.; Ko, M. S.; Niwa, H., *Nat Cell Biol* **2007,** *9* (6), 625-35. DOI 10.1038/ncb1589.
68. Klein, A. M.; Mazutis, L.; Akartuna, I.; Tallapragada, N.; Veres, A.; Li, V.; Peshkin, L.; Weitz, D. A.; Kirschner, M. W., *Cell* **2015,** *161* (5), 1187-201. DOI 10.1016/j.cell.2015.04.044.
69. Wu, A. R.; Neff, N. F.; Kalisky, T.; Dalerba, P.; Treutlein, B.; Rothenberg, M. E.; Mburu, F. M.; Mantalas, G. L.; Sim, S.; Clarke, M. F.; Quake, S. R., *Nat Meth* **2014,** *11* (1), 41-6. DOI 10.1038/nmeth.2694.
70. Deng, Y.; Zhang, N.; Zhao, L.; Yu, X.; Ji, X.; Liu, W.; Guo, S.; Liu, K.; Zhao, X. Z., *Lab Chip* **2011,** *11* (23), 4117-21. DOI 10.1039/c1lc20494g.
71. Lindström, S.; Andersson-Svahn, H., *Single-Cell Analysis: Methods and Protocols*. Humana Press: **2012**.
72. Di Carlo, D., *Microfluidic Technologies for Single-Cell Analysis*. VDM Verlag: **2009**; p 116.
73. Rettig, J. R.; Folch, A., *Anal Chem* **2005,** *77* (17), 5628-34. DOI 10.1021/ac0505977.
74. Chen, H.; Sun, J.; Wolvetang, E.; Cooper-White, J., *Lab Chip* **2015,** *15* (4), 1072-83. DOI 10.1039/c4lc01176g.
75. Chanasakulniyom, M.; Glidle, A.; Cooper, J. M., *Lab Chip* **2015,** *15* (1), 208-15. DOI 10.1039/c4lc00774c.

76. Lindstrom, S.; Eriksson, M.; Vazin, T.; Sandberg, J.; Lundeberg, J.; Frisen, J.; Andersson-Svahn, H., *PloS one* **2009,** *4* (9), e6997. DOI 10.1371/journal.pone.0006997.
77. Faley, S. L.; Copland, M.; Wlodkowic, D.; Kolch, W.; Seale, K. T.; Wikswo, J. P.; Cooper, J. M., *Lab Chip* **2009,** *9* (18), 2659-64. DOI 10.1039/b902083g.
78. Yu, L.; Chen, M. C.; Cheung, K. C., *Lab Chip* **2010,** *10* (18), 2424-32. DOI 10.1039/c004590j.
79. Shi, Y.; Gao, X.; Chen, L.; Zhang, M.; Ma, J.; Zhang, X.; Qin, J., *Microfluidics and Nanofluidics* **2013,** *15* (4), 467-474. DOI 10.1007/s10404-013-1160-6.
80. Tan, W.-H.; Takeuchi, S., *Adv Mat* **2007,** *19*, 2696–2701.
81. Dolega, M. E.; Abeille, F.; Picollet-D'hahan, N.; Gidrol, X., *Biomaterials* **2015,** *52*, 347-57. DOI 10.1016/j.biomaterials.2015.02.042.
82. Singer, Z. S.; Yong, J.; Tischler, J.; Hackett, J. A.; Altinok, A.; Surani, M. A.; Cai, L.; Elowitz, M. B., *Mol Cell* **2014,** *55* (2), 319-31. DOI 10.1016/j.molcel.2014.06.029.
83. Sun, Y.; Chen, C. S.; Fu, J., *Annu Rev Biophys* **2012,** *41*, 519-42. DOI 10.1146/annurev-biophys-042910-155306.
84. Watt, F. M.; Huck, W. T., *Nat Rev Mol Cell Biol* **2013,** *14* (8), 467-73. DOI 10.1038/nrm3620.
85. Ertl, P.; Sticker, D.; Charwat, V.; Kasper, C.; Lepperdinger, G., *Trends Biotechnol* **2014,** *32* (5), 245-53. DOI 10.1016/j.tibtech.2014.03.004.
86. Lesher-Perez, S. C.; Frampton, J. P.; Takayama, S., *Biotechnology Journal* **2013,** *8* (2), 180-91. DOI 10.1002/biot.201200206.
87. Filipczyk, A.; Marr, C.; Hastreiter, S.; Feigelman, J.; Schwarzfischer, M.; Hoppe, P. S.; Loeffler, D.; Kokkaliaris, K. D.; Endele, M.; Schauberger, B.; Hilsenbeck, O.; Skylaki, S.; Hasenauer, J.; Anastassiadis, K.; Theis, F. J.; Schroeder, T., *Nat Cell Biology* **2015,** *17* (10), 1235-46. DOI 10.1038/ncb3237.
88. Imamura, Y.; Mukohara, T.; Shimono, Y.; Funakoshi, Y.; Chayahara, N.; Toyoda, M.; Kiyota, N.; Takao, S.; Kono, S.; Nakatsura, T.; Minami, H., *Oncology Reports* **2015,** *33* (4), 1837-43. DOI 10.3892/or.2015.3767.
89. Buckingham, M. E.; Meilhac, S. M., *Dev Cell* **2011,** *21* (3), 394-409. DOI 10.1016/j.devcel.2011.07.019.
90. Blanpain, C.; Simons, B. D., *Nature reviews. Molecular Cell Biology* **2013,** *14* (8), 489-502. DOI 10.1038/nrm3625.
91. Feder-Mengus, C.; Ghosh, S.; Reschner, A.; Martin, I.; Spagnoli, G. C., *Trends Mol Medicine* **2008,** *14* (8), 333-40. DOI 10.1016/j.molmed.2008.06.001.
92. Krieger, T.; Simons, B. D., *Development* **2015,** *142* (8), 1396-406. DOI 10.1242/dev.101063.
93. Kalkan, T.; Olova, N.; Roode, M.; Mulas, C.; Lee, H. J.; Nett, I.; Marks, H.; Walker, R.; Stunnenberg, H. G.; Lilley, K. S.; Nichols, J.; Reik, W.; Bertone, P.; Smith, A., *Development* **2017,** *144* (7), 1221-1234. DOI 10.1242/dev.142711.
94. Mulas, C.; Kalkan, T.; Smith, A., *Stem Cell Reports* **2017,** *9* (1), 77-91. DOI 10.1016/j.stemcr.2017.05.033.
95. Kumachev, A.; Greener, J.; Tumarkin, E.; Eiser, E.; Zandstra, P. W.; Kumacheva, E., *Biomaterials* **2011,** *32* (6), 1477-83. DOI 10.1016/j.biomaterials.2010.10.033.
96. Zinchenko, A.; Devenish, S. R.; Kintses, B.; Colin, P. Y.; Fischlechner, M.; Hollfelder, F., *Anal Chem* **2014,** *86* (5), 2526-33. DOI 10.1021/ac403585p.
97. Nolting, J. F.; Koster, S., *New J Phys* **2013,** *15*. DOI Artn 045025 10.1088/1367-2630/15/4/045025.
98. Birol, S. Z.; Fucucuoglu, R.; Cadirci, S.; Yazgan, A. S.; Trabzon, L., *IEEE 12th International Conference on Nano/Micro Engineered and Molecular Systems* **2017**, 239-242. DOI 10.1109/NEMS.2017.8017015.